Revisiting copper as a case study of creep in pure metals: Prediction of creep response in pure Cu in half-hard and friction-stir-processed states

POST-PRINT (ACCEPTED COPY)

Revisiting copper as a case study of creep in pure metals: prediction of creep response in pure Cu in half-hard and friction-stir-processed states

C.Paoletti[a], E. Santecchia[b], M. Cabibbo[b], M. Regev[c], S. Spigarelli [b]

a. Faculty of Engineering, Università degli Studi eCampus, Via Isimbardi 10, 22060 Novedrate, Italy

b. DIISM, Università Politecnica delle Marche, via Brecce Bianche, 60131, Ancona, Italy

c Mechanical Engineering Department, ORT Braude College, P.O. Box 78, Karmiel, 2161002

https://doi.org/10.1016/j.msea.2021.142426

Received 23 September 2021; Received in revised form 25 November 2021; Accepted 26 November 2021

Available online 1 December 2021

Revisiting copper as a case study of creep in pure metals: prediction of creep response in pure Cu in half-hard and friction-stir-processed states

C.Paoletti[a], E. Santecchia[b], M. Cabibbo[b], M. Regev[c], S. Spigarelli [b]

a. Faculty of Engineering, Università degli Studi eCampus, Via Isimbardi 10, 22060 Novedrate, Italy

b. DIISM, Università Politecnica delle Marche, via Brecce Bianche, 60131, Ancona, Italy

c Mechanical Engineering Department, ORT Braude College, P.O. Box 78, Karmiel, 2161002

Abstract

A physical model was used to obtain a pre-assessment of the dependence of minimum creep rate on stress and temperature for ETP copper under two different initial conditions, *i.e.*, in the R240 half-hardened state and after friction stir processing. Although the R240 samples contained a high dislocation density owing to pre-straining, the material that underwent friction stir processing (FSP) had a much finer grain size and a far lower dislocation density.

The original Sandström physically based model developed for copper was modified to take into account the strengthening role of the grain boundaries, and its declining importance with increasing temperature and/or decreasing applied stress. In addition, the grain growth effect was estimated using appropriate empirical equations. The model curves obtained by introducing a few initial information, such as the grain size and the ultimate tensile strength at room temperature, in the resulting set of constitutive equations, largely overlapped. This finding was somewhat in conflict with the traditional view, which assumes that a fine grain size is an ineffective source of creep strengthening, if not detrimental.

Subsequent creep experimental testing carried out between 178 and 355 °C substantially confirmed the picture provided by the pre-assessment, and the minimum creep rate values for the two materials

largely overlapped on the same curves. Only at 355 °C did the FSP samples exhibit a somewhat higher creep rate, when compared with the R240 samples and the pre-assessment curve. The experimental data obtained for R240 copper at 475 °C were not properly described by the physical model, as expected on the basis of the previous literature reports.

Keywords: creep; copper; plasticity; constitutive equations.

1. Introduction

Pure copper, from a historical point of view, was one of the first materials to be investigated to shed light on the creep-controlling mechanisms [1-6] (interested readers can find a summary of a wider selection of less recent literature results in ref.[3]). More recently, there has been a renewed interest in this metal owing to applications of pure Cu in the storage of nuclear waste. This is because creep can occur even in the low-temperature range relevant to the waste package. This new effort resulted in the elaboration, made by Sandström and co-workers [7-11], of a physically based model (synthetically illustrated in a slightly modified and simplified form in Section 2 of the present paper) which does not require fitting of experimental data to predict the material creep response. This predictive capability could constitute a significant advancement over phenomenological approaches. The traditional description of the minimum creep rate ($\dot{\varepsilon}_m$) dependence on the applied stress (σ) and absolute temperature (T) [12] is expressed by the universally known equation:

$$\dot{\varepsilon}_m = A\frac{DGb}{kT}\left(\frac{\sigma}{G}\right)^n \qquad (1)$$

where b is the Burgers vector, G is the shear modulus, A is a constant, n is the stress exponent, $D=D_0\exp(-Q/RT)$ is the appropriate diffusion coefficient, Q is the creep activation energy, and D_0 is a constant. In pure metals, for a wide range of temperatures and applied stresses, creep is said to be mostly climb-controlled, and Eqn. (1) works well. In such a case, D should be equivalent to the coefficient for vacancy diffusion $D_L=D_{0L}\exp(-Q_L/RT)$, i.e. $D_0=D_{0L}$ and $Q=Q_L$ (see Table I for the meaning of the symbols). On the other hand, at low temperatures/high stresses, power law breakdown requires the substitution of Eqn. (1) with the other models. In addition, for copper above 400°C, the experimental values of the apparent activation energy

$$Q_a = -R\left.\frac{\partial ln\dot{\varepsilon}_m}{\partial(1/T)}\right|_{\sigma/G} \quad \text{or} \quad Q_a = -R\left.\frac{\partial ln\dot{\varepsilon}_m}{\partial(1/T)}\right|_{\sigma} \qquad (2)$$

are much lower than the activation energy for self-diffusion [3,5,13], which is close to 200 kJ mol^{-1} [14]. Raj and Langdon [3] reported a decrease in the apparent activation energy for creep with increasing stress, from 180 to 130 kJ mol^{-1}. Wilshire and Battenbough reported an even lower

activation energy (110 kJ mol^{-1}) [13]. These reductions in the activation energy were accompanied by a substantial change in the pre-exponential factor D_0.

This behaviour has been discussed at length by many authors (see refs.[3,5,13]). However, one of the major problems, the essentially phenomenological nature of the most widely used creep models, remains largely unresolved, particularly when advanced technologies, such as friction stir processing, are used to modify the initial microstructure.

Friction stir processing (FSP) is a technique derived from the friction stir welding (FSW)[15]. In FSP, the rotating tool does not weld two parts, but causes a severe plastic deformation and heating of a single plate. The combination of deformation and heating leads to recrystallisation in the stir zone, resulting in a very fine grain size. Many different aspects of the microstructure and mechanical properties of Cu processed by FSP have been investigated in a number of studies (see refs.[16-20]), but the possible effect of the very fine initial microstructure on creep remains to be discussed. In this context, the present paper aims at a two-fold scope:

i. To test the predictive capabilities of the physically based model developed in the refs. [7-11] by obtaining a pre-testing assessment of the creep behaviour, i.e., an a-priori evaluation of the material response before the experiments are carried out. The material considered was ETP copper with two different initial microstructures: a half-hardened plate (R240 state) and the same material after FSP (FSP state). Based on the well-established beliefs, such as the predominance of creep in the effect of a high dislocation density over the strengthening role of grain boundaries, one could preliminarily conclude that the R240 strain-hardened material should exhibit, at least in the low-temperature regime, a low creep rate under a given stress than that of the softer recrystallised FSP copper. The results of the pre-assessment will be compared with this early and superficial analysis. This section of the study is addressed in Section 2.

ii. To experimentally evaluate the effect of these differences in the initial microstructure on creep in a temperature range which is intermediate between the low-temperature regime investigated in refs.[7-11], and the high temperature range considered in refs. [3,13] (Sections 3 and 4). The

experimental data were then used in a cascade to validate the pre-assessment of the creep response of the considered materials (Section 5). The resulting discussion led to revisiting the concept of copper as a good case study for the creep of pure metals, demonstrating that past interpretations of the role of different creep-controlling mechanisms should be reconsidered starting from more detailed microstructural investigations.

2. Pre-testing assessment of the creep response of fine-grained pure Copper

Copper has been extensively investigated as one might expect to have sufficient information to predict the material response at high temperatures. In principle, one would need to collect enough literature evidence to obtain a coherent picture of the material response in the form of reliable constitutive equations. These equations may then be used to obtain a pre-assessment of the creep response of ETP copper in the intermediate temperature range considered here (178 – 475 °C). In the present study, the minimum or steady-state creep rate obtained in constant-load/stress experiments, *i.e.*, without any change in the load during the test, as a function of temperature and stress, will be predicted for both R240 and FSP-processed copper. To maintain the possibility of validating the pre-assessment, the temperatures considered will be the same as those used in the experimental part of the study (178, 252, and 355 °C). An additional temperature (475 °C) was also considered for the R240 metal.

2.1 Constitutive model

The prediction of the creep rate dependence on stress and temperature for pure copper can be carried out using the physically based model proposed by Sandström et al. [7-11]. The model is based on the well-known Taylor equation, which is rewritten in a form which slightly differs from the original one of refs. [7-11], i.e.,

$$\sigma = \sigma_{0i} + \frac{k_{HP}(T,\dot{\varepsilon})}{\sqrt{d(T,t)}} + \alpha m G b \sqrt{\rho} \qquad (3)$$

or

$$\sigma_\rho = \alpha m G b \sqrt{\rho} = \sigma - \sigma_{0i} - \frac{k_{HP}(T,\dot{\varepsilon})}{\sqrt{d(T,t)}} \quad (4)$$

where m is the Taylor factor, σ_{0i} represents the stress required to move a dislocation in the absence of other dislocations in a very coarse-grained metal, d is the grain size, which is a function of time and temperature; k_{HP} is the temperature- and strain-rate-dependent Hall-Petch constant, and α is a constant (Table I). Equation (4) differs from the original formulation employed in refs. [7-11], because the Hall-Petch strengthening term is explicitly quantified, even though, as will be discussed later, the effect of the grain size is seldom considered to have any significance in climb-controlled creep.

The evolution of the dislocation density during straining at high temperature can be expressed (Appendix 1) as

$$\frac{d\rho}{d\varepsilon} = \frac{m\sqrt{\rho}}{bC_L} - \frac{2}{\dot{\varepsilon}} M \tau_l \rho^2 \quad (5)$$

where τ_l is the dislocation line tension (τ_l=0.5Gb^2), M is the dislocation mobility, and C_L is the strain-hardening constant. The dislocation mobility is given by

$$M = \frac{Db}{kT} exp\left(\frac{\sigma_\rho b^3}{kT}\right) exp\left\{\frac{Q}{RT}\left(\frac{\sigma_\rho}{R_{max}}\right)^2\right\} \quad (6)$$

where D is the appropriate diffusion coefficient, and Q is the corresponding value of the activation energy for the rate-controlling mechanism. As mentioned above, for climb-controlled creep, D=D_L, and Q=Q_L. Thus, the equation becomes:

$$M = \frac{D_{0L}b}{kT} exp\left(\frac{\sigma_\rho b^3}{kT}\right) exp\left\{-\frac{Q_L}{RT}\left[1 - \left(\frac{\sigma_\rho}{R_{max}}\right)^2\right]\right\} \quad (7)$$

where R_{max} is the true stress corresponding to the ultimate tensile strength of the material.

Combination of Eqns.(5) and (7), at the steady-state yields (see Appendix 1 for derivation)

$$\dot{\varepsilon}_{ss} = \frac{2\tau_l D_{0L} b^2 C_L}{mkT}\left(\frac{\sigma_{\rho ss}}{\alpha m G b}\right)^3 exp\left(\frac{\sigma_{\rho ss} b^3}{kT}\right) exp\left\{-\frac{Q_L}{RT}\left[1 - \left(\frac{\sigma_{\rho ss}}{R_{max}}\right)^2\right]\right\} \quad (8)$$

where $\sigma_{\rho ss}$ is the dislocation strengthening term corresponding to the equilibrium dislocation density at the steady state or in the minimum creep rate range. Full details of the derivation of Eq.(8) can be found in refs. [7-11].

2.2 Grain strengthening effect and its variation with temperature and strain rate

The temperature- and strain-rate dependence of the Hall-Petch parameter k_{HP} can be expressed by the following empirical equation [21]:

$$k_{HP}^2 = B_{HP} exp(-\beta_{HP} T) \quad (9)$$

where B_{hp} is a constant and

$$\beta_{HP} = \beta_0 - \beta_1 ln\dot{\varepsilon} \quad (10)$$

with β_0 = 0.00355 K^{-1}, β_1=2 × 10^{-4} K^{-1} for Cu [21,22], the strain rate being given in s^{-1}. The constant B_{HP} was calculated from the k_{HP} *vs.* temperature plot presented in ref. [22], based on the data obtained in ref. [23] for a strain rate of 6.7 × 10^{-4} s^{-1}, obtaining B_{HP} = 91 $MPa^2 \cdot mm^{-1}$.

To properly quantify the Hall-Petch strengthening effect, if any exists, an estimate of *d* at the time corresponding to the minimum creep rate must be obtained. The identification of the correct law for grain growth is well beyond the scope of the present study, but ultrafine grains are known to grow even at relatively low temperatures (see refs. [24,25]). Thus, following Ghauri et al. [26] the law

$$d^2 = d_0^2 + k_{GG} exp\left(-\frac{Q_{GG}}{RT}\right) t \quad (11)$$

where d_0 is the initial grain size, *t* is time, Q_{GG} is the activation energy for the grain growth, and k_{GG} is a material parameter. Table II lists a collection of measured k_{GG} and Q_{GG} values obtained from the literature, which correspond to very different kinetics of grain growth, which poses an obvious problem in identifying the proper law. Alternatively, one could attempt to calculate the k_{GG} and Q_{GG} values by assuming $Q_{GG} = Q_{GB}$, where Q_{GB} is the activation energy for grain boundary diffusion, and that from ref. [24]

$$k_{GG} = \frac{4\gamma\Omega D_{0GB}}{\delta kT} \quad (12)$$

where Ω is the atomic volume, δ is the grain boundary width, γ is the grain boundary surface energy, and D_{0GB} is the pre-exponential constant in the expression for the grain boundary diffusion coefficient. Table III presents a few examples of the D_{0GB} and Q_{GB} values available in the literature. Again, as in the case of Table II, the selection of the different values of the parameters listed in Table III results in very different grain growth kinetics. The large variation in the predicted kinetics of grain growth is a problem that represents a serious obstacle to obtaining a reliable pre-assessment. Nevertheless, the accuracy of most of these estimates of grain growth in the considered range of temperatures (178 – 355 °C) can be seriously questioned since the grain size they provide is greatly exaggerated. On this basis, the growth law that resulted in the slowest increase in grain size (k_{GG}= 3.6 × 10^{-8} m^2s^{-1}, Q_{GG}=82 kJ mol^{-1}) was tentatively assumed to provide the most reliable estimate of the grain growth.

2.3 Pre-assessment of the minimum creep rate dependence on applied stress and temperature

Sections 2.1 and 2.2 describe the set of constitutive equations that will be used to predict the creep response of pure copper in the half-strain-hardened R240 state and after FSP.

For the pre-assessment, the first assumption introduced here is that the value of the minimum creep rate depends on the grain size, stress, temperature, and R_{max}, while other aspects of the initial microstructure (mainly the initial dislocation density) affect the mode through which this value is reached, i.e., the strain upon loading and the shape of the primary creep curve. Few other parameters need to be estimated, namely,

i. The initial grain size;

ii. The R_{max} parameter. This parameter can be calculated by the equation [30]

$$R_{max} = 1.5\ UTS\ \frac{G_T}{G_{RT}} \quad (13)$$

iii. The stress required to move a dislocation in the absence of other dislocations in a very coarse-grained metal (σ_{0i}). For copper, a material with a very low Peierls stress τ_P (τ_P/G

$< 0.7 \times 10^{-5}$) [31], the modulus-compensated critical resolved shear stress (τ_{CRSS}/G) is close to 1.2×10^{-5} at room temperature [32]. The critical resolved shear stress exhibits a dependence on the strain rate and temperature in the range of experimental conditions investigated in [32]. However, for the sake of simplicity, one can reasonably assume that the magnitude of the modulus-compensated critical resolved shear stress remains constant in the range of temperatures considered in the present study. This term is completely negligible at low and medium temperatures when high applied stresses are needed to obtain noticeable creep rates but could become significant at higher temperatures in the low-stress regime. Based on this, a constant value of $\sigma_{0i}/G = m\tau_{CRSS}/G \cong 3.6 \times 1\ 0^{-5}$ was assumed in all the considered ranges of temperatures and strain rates.

Figure 1 plots a family of strain rate *vs.* stress curves calculated for different combinations of values of the grain size (3 and 30 μm) and of the tensile strength (200 and 300 MPa). To clearly separate the effects of UTS and grain size, it was here assumed that grain size remains stable during creep (no grain growth). Equations (8) and (13) thus predict that a material with a higher UTS will exhibit a lower strain rate than a similar metal with lower UTS tested under the same external stress. This, in turns, implies that the material with higher UTS, at steady state, will require a higher $\sigma_{\rho ss}$ to creep at a given strain rate, i.e., a higher dislocation density will be observed in that condition. On the other hand, for the peculiar formulation of the constitutive equation, the difference progressively disappears for low applied stresses (long test duration and/or high temperatures). In parallel, a decrease of the grain size, according to the above-described model, results in a substantial reduction of the minimum creep rate.

Grain growth, not considered in Fig.1, could be expected to dramatically decrease the grain size effect for low stresses (long test durations) at high temperatures. Thus, a fourth parameter needs to be estimated, namely:

iv. the time t_m corresponding to a given minimum creep rate $\dot{\varepsilon}_m$. This last parameter is crucial because it is necessary to predict the grain size corresponding to the minimum creep rate range. Although this value is required for the pre-assessment, in principle, it is not available before carrying out new experiments, but can be obtained from literature data. In the present instance, it can be assumed that [30] for tests carried out under a constant stress or load until the tertiary stage is initiated.

$$t_m = \frac{c_m}{\dot{\varepsilon}_m} \qquad (14)$$

being c_m =4.89 ×10^{-2} (from the curve at 250 °C,90 MPa in [9]).

The initial grain size for the R240 material was assumed to be 10 μm The FSP was considered to produce a very fine grain size, which was tentatively estimated at 3 μm. The UTS values were 285 and 235 MPa for the parent R240 plate and the FSP-processed material, respectively (information on experimental grain sizes and UTS is given in Section 3).

All parameters needed for pre-assessment are now available. In the case of the materials considered in the present study, where grain growth is expected to occur, the true stresses for minimum creep rates decrease from 2.7 × 10^{-3} s^{-1} down to 2.7 × 10^{-9} s^{-1}, which corresponds to t_m ranging from 18 s to 5000 h, Eqn.(14), were iteratively calculated using Eqs. (8), (9), (10), (11) and (13). Figure 2 plots the curves obtained by connecting the resulting data points and provides a pre-assessment of the creep response for R240 and FSP-processed metals. The analysis of the figure suggests that, according to the pre-assessment, for the considered initial states, the effects of the different initial strengths and grain sizes are barely noticeable. The difference in UTS between the two considered conditions is thus largely compensated by the Hall-Petch strengthening term, which defies the probably simplistic view that a fine grain size is always undesirable in creep.

If the pre-assessment based on the model discussed in this section is correct, the experimental data obtained by testing the material in the R240 and FSP states should thus substantially overlap on the same curves. The accuracy of this pre-assessment and the resulting implications will be discussed in a later section.

3. Experimental procedure

3.1 Materials

The material tested in the present study was a commercial 3 mm-thick plate of Cu-ETP in the R240 half-hard condition. The material underwent FSP at a rotational speed $\omega = 900$ rpm and a transverse speed of $v = 50$ mm/min. A single pass was made on one side of the plate, which was then reversed and processed once again immediately above the first pass. Following this approach, the advancing side of the first pass became the retreating side of the second pass, and vice versa, leading to a uniform and almost rectangular cross-section of the stir zone. Tensile tests were carried out under a strain rate of 1.3×10^{-4} s^{-1} on both the as-received and FSP materials. Table IV summarises the results of the six tensile tests for each condition. Details on the microstructure of the as-received and FSP materials can be found in ref.[33], so only a few details will be recalled here. The grain size of the FSP-processed material (a few microns) was much finer than that of the parent metal, whose grains ranged in size from 5 to 20 μm. In addition, transmission electron microscopy (TEM) study of the FSP samples highlighted the existence of nanosized grains formed during dynamic recrystallisation (DRX).

The TEM study also revealed that, as expected, the material in the R240 state contained a high dislocation density. Although the FSP metal contained a non-negligible dislocation content, it remained much lower than that of the R240 state. This resulted in a lower dislocation hardening effect, which was not fully compensated in the FSP state by the finesse of the grain size, so its room temperature mechanical properties (Table IV) were only marginally superior to copper in the annealed state (UTS close to 200 MPa). In addition, the hardness distribution in the FSP zone was

inhomogeneous. The micro-hardness ranged between 80 and 90 HV in the central zone of the stir zone, an effect that could be attributed to the many complex metallurgical phenomena occurring in parallel during FSP.

3.2 Experimental details

Two sets (half-hard R240 and FSP) of dog-bone samples, 25 mm in gauge length and 3 mm × 3 mm square section, were creep-tested at 178, 252, and 355 °C in constant-load machines. In the case of the FSP plate, the sample was machined with the specimen axis centred along the processed zone. Thus, the entire gauge length was constituted by the material transformed by the FSP. A few additional tests were carried out at 475 °C on samples machined from the R240 plate.

The temperature was measured during the tests using three thermocouples to reach a ±1°C homogeneity of the temperature along the sample. Elongation was measured using an LVDT and continuously recorded.

Two different types of creep tests were carried out: i) Constant-Load Experiments (CLE), during which the sample was maintained under a constant load until completion of the test (rupture or interruption well in the tertiary region); ii. Variable Load Experiments (VLE). In VLE, the load was changed during the test, in principle, after a reasonably constant strain rate, i.e., the minimum creep rate range, was attained. The change in load could be repeated during the test, thus obtaining multiple values of the presumed minimum creep rate values for a single experiment. Because high strains were usually accumulated before the samples reached the minimum creep rate range, the true stress σ is expressed as

$$\sigma = s(1 + e + e_i) \qquad (15)$$

where e is the engineering creep strain accumulated during the test, and e_i is the instantaneous elastic/plastic engineering strain upon initial loading, assuming considerably higher values than the initial (nominal) stress s.

TEM was used to detect the possible presence of secondary phases and to characterise the substructure of the material under different experimental conditions.

To this purpose, TEM discs were prepared mechanically by polishing thin foils down to a thickness of 120 μm, followed by punching to a 3 mm diameter and then dimpled to produce a double-sided spherical pit with a central thickness of 30 μm. Final thinning to electron transparency was obtained by using a Gatan™ precision ion-milling (PIPS) working at 8 V and incident beam angle of 8-to-4°. A PhilipsTM CM20® operated at 200 keV and equipped with a nitrogen-cooled double-tilt specimen holder was used to perform TEM inspections. Selected area electron diffraction patterns were recorded by converging the electron beam.

4. Experimental results

4.1 Creep tests

Tables V and VI summarise the experimental results from the CLE and VLE for the R240 and FSP conditions. Figure 3 shows the representative examples of the curves obtained from the CLE experiments at 178 and 252 °C. The figures compare the curves for the R240 and FSP materials tested under the same initial nominal stress, *s*.

Figure 4 presents other examples of creep curves (in strain rate *vs*. strain form) for the two investigated conditions. Figure 5 shows examples of the creep curves obtained by testing the AR metal at 475 °C (no experiments were performed at this temperature for the FSP metal, owing to the presumed microstructure instability of the fine-grained microstructure). The shape of the curves at this temperature is slightly different, as a rapid increase in the strain rate is observed just after the minimum creep rate range (see, in particular, the test under 35 MPa).

The FSP material is softer and undergoes a much larger instantaneous and primary creep strain, and its minimum creep rate is higher than that of the R240 material tested under the same initial stress, if only because of the higher value of the true stress.

These differences influence the shape of the creep curve that can be obtained in the R240 and FSP samples tested under the same initial stress. Two different behaviours are observed.

a. Curve of type I: A sharp decrease in the strain rate is followed by a minimum creep rate range, followed by a tertiary region which leads to rupture at relatively low strains. The minimum creep rate is observed below $\varepsilon = 0.02$. This behaviour is typical of the samples tested under initial stresses well below yielding (tests at 252 °C,120 MPa for R240 and 355°C,55 MPa, for both R240 and FSP).
b. Curve of type II: The strain rate gradually decreases until the minimum creep rate range is reached at a strain above 0.1. This behaviour is typical of samples tested close to or above yielding.

In many of the FSP samples, characterised by large primary strains, the creep curve is type II. Few experiments, carried out at low applied stresses, exhibit curves of type I. In contrast, in R240 samples, type I curves can be more frequently observed and, in any case, the instantaneous strain upon loading is lower.

Figure 6 shows the hardness measured on the crept R240 sample heads, i.e., in lowly stressed portions of the specimen, tested at different temperatures (the soaking time was not considered). Hardness was measured on the heads and not along the gauge length to avoid the effect of the additional dislocation density introduced during loading. During ageing, the hardness did not decrease at 178 and 252 °C, and only slowly decreased at 355 °C. In contrast, at 475 °C, the hardness decreases to low values just after 1000 s (plus soaking time), a clear indication of the occurrence of recrystallisation upon heating.

4.2 Microstructure of crept samples

Figure 7 shows representative micrographs of the microstructure of the samples after creep, and also reports the predicted grain size (Section 2). Grain growth surely occurs during creep, but even

the formulation for the slowest kinetics law provided in Section 2.2 seems to somewhat overestimate this effect for long time of exposure.

TEM inspections focused on the microstructural evidence to verify possible sources of strengthening, not expressly considered in the current models, namely the presence of secondary phase and/or oxide particles. Figure 8, which shows the microstructure of the two samples observed by TEM, confirms the presence of remote rounded particles, identified as Cu_2O by SAEDP. The presence of such fine oxide particles was clearly detected on the head of the sample tested at 355 °C for 23 h (Figure 8a), as well as in the gauge length of the R240 material crept at 475 °C (VLE, tested under 20 and 41 nominal stresses, overall test duration 170 h) (Figure 8b). These oxides were mostly detected at triple junction points and in grain boundary regions and were usually within 100 nm in size (mean equivalent diameter of 80 ± 10 nm). Due to the limited number of such oxide particles detected, no statistical evaluation of their volume fraction was possible in either sample.

5. Discussion

5.1 Analysis of the creep response of the half-hardened and friction-stir-processed materials: creep curves

Attaining measurable creep rates in this range of temperatures requires the use of high stresses. As a result, the softer FSP material mostly undergoes plastic straining upon loading and continuously hardens until the minimum creep rate range is reached at high strains, giving, in most cases, type II curves. The situation is different in the harder R240 material. The half-hard state can be obtained by applying skin-pass cold rolling to an annealed plate [34]. The skin-pass imparts a moderate strain hardening, that is roughly quantifiable as a 10-20% cold work [34,35]. The dislocation density corresponding to such a prestrain level could range from approximately 3.0×10^{14} m^{-2} [36] to 1.0×10^{15} m^{-2} [37]. Heating at the testing temperature, at least between 178 and 355 °C, marginally affects the initial dislocation density because of its short soaking time before the loading (max. 30 min). This is clearly demonstrated in Figure 6. Thus, a nominal stress *s*, that causes a measurable

plastic straining upon loading in the FSP metal, can be too low to generate any plastic straining in the hard R240 samples. When the nominal stress *s* is below yielding, the loading strains are predominantly elastic. In this case, the extent of the primary strain is reduced because the dislocation movement is limited by the prestrain-imposed substructure, and even the minimum creep rate could assume lower values (curves of type I) [13]. A type II curve, representing a slow decrease in creep rate until a minimum is reached at creep strains of 0.1 or above, is again observed only when the applied stress is sufficiently large, i.e., close or above yielding. The curves in Figure 5, obtained from samples greatly softened by exposure at 475 °C, invariably exhibit a type II shape, albeit they present a different shape of the tertiary stage, with a rapid increase in creep rate just after the minimum creep rate range.

5.2 Analysis of the creep response of half-hardened and friction-stir-processed materials: minimum creep rate dependence on applied stress

A comparison of the curves obtained for R240 and FSP metals under the same initial stress (Figure 3) is useful, since a preliminary conclusion about the differences in constant-load creep response under similar nominal stresses can be reached. However, as far as the study of the creep mechanisms is concerned, the minimum creep rate should be analysed as a function of the true stress, Eq.(15), rather than as a function of the initial (nominal) stress. Figure 9 presents the results for the R240 and FSP materials (open symbols represent data obtained by VLE), where the true stress is calculated in correspondence of the middle of the minimum creep rate range, i.e. at time t_m. Figure 9c compares the two datasets in the same plot. The analysis of the figures is extremely interesting because it shows that in most of the investigated range of temperatures and strain rates, the experimental data partly overlap on the same curve. As a result, if tested under constant stress conditions, the creep responses of the two investigated states should be very similar, as suggested by the pre-assessment. In general terms, the R240 material is more creep resistant—at a given true stress—at 355 °C in the low strain rate regime; however, in the rest of the experimental envelope,

the two conditions are essentially equivalent. By contrast, significant data scatter can be observed, particularly for the FSP samples, a hardly surprising behaviour when considering the large hardness variations in the stir zone [33].

Figure 10 plots the time to minimum creep rate t_m as a function of the minimum creep rate at 178, 252 and 355 °C. Most of the data roughly align on the same straight line, i.e., on the curve identified by Eqn.(14). Only a small group of the data, all for R240 metal, align on a different line that corresponds, for a given strain rate, to lower values of t_m. Figure 11 provides an explanation for this behaviour. The Figure 11 plots the range of yield stress and UTS for Cu in the annealed state, as a function of the testing temperature, obtained by a collection of different data [13,23,38,39]. The Figure 11 also plots the yield strength for a sheet cold worked up to 6% and the UTS for a pure Cu rod after 21% cold work [39]. The Figure 11 suggests that heating above 300 °C for a sufficiently prolonged duration, causes the progressive loss of strength of the cold-worked state, which, above 400 °C, due to extensive recrystallisation, becomes roughly equivalent to the annealed state. On the other hand, when one compares the high yield stress values of the 6% cold-worked sheet at temperatures below 200 °C, with the initial stresses of the tests which deviates from Eqn.(14), a straightforward conclusion could be that these tests did not show significant plastic deformation upon loading. Figure 10 thus simply illustrates another aspect of the behaviour shown in Figure 3. The experiments which roughly align on the curve given by Eqn.(14), corresponds to type II creep curves. By contrast, the data points which align on the lower straight line, were obtained from the type I curves (experimental stress well below yielding).

Consistently, the extensive plastic strain which occurs even under low stresses upon loading at 475 °C in the AR metal, is the result of the dramatic decrease in strength of the cold-worked material when the temperature exceeds 400 °C. Thus, an initial applied stress of 20 MPa is sufficient to cause a noticeable plastic strain.

5.3 Comparison between the pre-assessment curves and experimental data

The plot in Figure 12 is a direct comparison between the model curves obtained in Section 2, and the experimental data. In case of the metal in R240 state, there is an excellent agreement between the model and the experiments. Only under low applied stresses, at 355 °C, the model curve slightly overestimates the minimum strain rate. The situation is different at 475 °C, where the model curve greatly overestimates the creep rate in the whole regime of experimental conditions (this case will be briefly addressed in Section 5.3).

A similar pattern can be observed for the FSP metal. Again, a good correlation between the model and the data is obtained, except in the very low-stress region, although the effect of experimental scatter should be accounted for. However, while the model curves overestimate the creep rate in the R240 state, the situation is opposite for the FSP metal, that is, where the model tends to underestimate the creep rate.

An interesting point to be discussed now is the effect of the grain size on the dislocation creep regime. This aspect has been analysed by Wilshire and Palmer [40] and Kral et al. [41]. The traditional picture that dislocation creep is not affected by grain size, in particular, has been partly revised in [40], since Wilshire and Palmer observed that a decrease in grain size can result in a decrease in the creep rate, until a critical value d_{cr} is reached. As the grain size further decreases below d_{cr}, a more active role in the grain boundary zone should lead to an increase in the creep rate. Thus, a non-monotonic dependence of the minimum strain rate on the grain size was obtained. In addition, the effect of the ultrafine grain sizes on the creep response of pure Cu remains to be clarified. Earlier studies have reported examples in which the minimum creep rate of the **u**ltrafine-grained (UFG) Cu processed by eight passes in the Equal Channel Angular Pressing (ECAP) is higher (by a mere factor of two at 300 °C [42] or by more than two orders of magnitude at 200 °C [43]) when compared with coarse-grained (CG) material. On the other hand, a more recent study [41] confirmed that the minimum creep rates of UFG and CG copper were almost equivalent at

300°C. The same study revealed that at 100°C, the minimum creep rate of the UFG material was far lower than that of the CG metal. As a whole, the effect of a UFG structure on creep reported in ref. [41] is qualitatively similar to that observed in the present study, where a fine grain size roughly compensates for the effect of a by far higher initial dislocation density, which is consistent with the pre-assessment of the creep response.

The relevance of high-angle boundaries as obstacles to the movement of lattice dislocations was expressed in this study by introducing a strain rate and temperature-dependent Hall-Petch strengthening term. This fact explains why the much softer fine-grained material (substantially comparable to the hardest examples of annealed copper) exhibits a creep response which is almost equivalent to that observed on the same metal in a strain-hardened condition. Although the recovery at these temperatures is sluggish, it partly mitigates strain hardening, which is almost compensated by grain boundary strengthening. We can reasonably conclude that grain size, at least in the low temperature regime, has some relevance in determining the creep response, while it becomes substantially irrelevant at high temperatures. On the other hand, the Hall-Petch strengthening term has been quantified in Section 2.2, by merely using empirical equations. These formulations were obtained by experiments carried out in a regime of strain rate much higher than those typical of creep. In addition, the grain growth law also provides a strongly oversimplified picture of the much more complex phenomena which occur in the real microstructure [44] and, as a whole, the resulting estimate of the grain size in correspondence of the minimum creep rate range is, least to say, quite imprecise. On this ground, the relative accuracy of the pre-assessment is even somewhat surprising, being based on oversimplified descriptions of several different important parameters, such as the grain size, the Hall-Petch constant and, least but not the least, the σ_{0i} term. This further confirms that the Sandström model has a great potential if properly tuned with the correct physical laws.

As mentioned above, in this paper the grain boundaries are only considered as passive barriers for dislocations and are assumed to play no active role in either dislocation production or recovery. If the grain boundaries behave differently, that is, they are involved in the recovery process, the grain

size could explicitly appear in new forms of the equation describing the dislocation density kinetics. Such a development is worth of further analysis, which on the other hand falls well beyond the scopes of the present study.

5.4 Creep response above 400°C

The analysis of Figure 12, as mentioned above, demonstrates that the basic form of the model cannot be used to predict the material behaviour above 400°C. The model accurately describes the variation in the slope of the strain rate *vs.* stress curves but provides $\dot{\varepsilon}$ values that are one order of magnitude higher than the experimental values. This behaviour, already reported in refs. [8,11] is usually attributed to a change in the apparent activation energy with temperature. This phenomenon has not been fully understood [11], *e.g.*, in the case of aluminium, the Sandström model provides an excellent description of the creep data at temperatures ranging from 0.3 to 0.9 T_m, where T_m is the absolute melting point [30], with $D=D_L$. In copper, between 0.4 and 0.6 T_m, the calculated apparent activation energy for creep is much lower than Q_L and increases at higher temperatures, and, as a whole, the variation of the apparent activation energy is non-monotonic [45].

The material above 350°C is actually more creep resistant than the model prediction with $D=D_L$. Thus, at these high temperatures, the vertical separation between the isothermal curves in a double logarithmic plot of the strain rate as a function of the applied stress, which is associated with the apparent activation energy for creep, is lower than at 100 – 300 °C. This observation led to the replacement of Eq.(1) with other relationships that are valid at intermediate temperatures, which contain a lower activation energy [3,5,13]. Nevertheless, at higher temperatures, the apparent activation energy should again increase, which cannot be described by these new equations.

While different explanations have been proposed for the stress-dependent apparent activation energy (see refs. [3,5]) and the difference in behaviour between pure Cu with varying contents of impurity, no definite conclusion on rate-controlling dislocation mechanisms can still be drawn, since multiple and synergic factors, usually neglected, should be taken into account:

i. Dynamic recrystallisation (DRX): DRX could play a role, particularly at high temperatures. Without going into the details of the discussion on this subject, one can observe that the critical strain for the onset of DRX (ε_{cDRX}), as obtained in constant-strain-rate experiments, depends on both the strain rate and temperature. Extrapolation in the low strain rate regime of the critical strain for DRX obtained in ref. [46] at 400°C suggests that the critical strain for DRX at 475 °C is lower than that for the minimum creep rate. The results obtained in constant-strain-rate tests should be carefully used when interpreting creep curves, where the strain rate changes with strain. Nevertheless, these findings seem to indicate that, at least in the half-hard state tested at this temperature, after the first wave of static recrystallisation (SRX) occurred during heating and soaking time, DRX indeed occurred during creep. This should lead to a new softening wave of the microstructure, partly compensated by the effect of an ultrafine recrystallised microstructure which later undergoes grain growth, possibly giving the peculiar shape of the tertiary creep in Figure 5, different from those observed at lower temperatures. This picture, mutatis mutandis, is qualitatively consistent with ref.[47]. Gottstein observed that during tensile straining of the Cu-single crystals, the occurrence of DRX took place in the secondary region at very high temperatures, while the recrystallisation that commenced before the deformation became stationary at lower deformation temperatures. DRX has indeed been frequently invoked to explain very high values of the apparent activation energy for creep at very high temperatures (see ref. [3] for a summary in this regard), although this phenomenon should result in a decrease in the material strength, which is not the case for high-temperature data for Cu.

ii. Particle strengthening by oxides: The effect of oxygen has been almost invariably neglected, but it has recently been suggested that it significantly influences the mechanical properties at high temperatures [48,49]. In particular, the increase in the oxygen content from 26 to 62 ppm corresponded to an increase in the apparent activation

energy for deformation above 600 °C from 216 to 278 kJ mol^{-1}, respectively, with a parallel increase in the peak flow stress of the stress vs. strain curves. This effect was attributed to the dynamic precipitation of fine nanosized and semi-coherent Cu_2O, which was evident at 750 °C in copper with 62 ppm of oxygen [48,49]. The formation of these oxide particles during deformation should be observed in a limited range of temperatures because of the high oxygen solubility above 800 °C and sluggish precipitation kinetics below 350 °C.

iii. Solid solution strengthening: Solid solution strengthening was observed in the OFP copper containing 60 ppm phosphorus. The interaction between the P atoms and dislocations resulted in an increase in activation energy from 198 to ≅ 206 kJ mol^{-1} at 75–150 °C [10]. The high P content in the materials described in ref. [49] (297 and 153 ppm in copper containing 26 and 62 ppm oxygen, respectively) contribute to solid solution strengthening. Nevertheless, the lower P content in the material richer in oxygen, which had a much higher apparent activation energy for high temperature deformation, suggests that in this case, the solid solution should be less effective than oxides in increasing the material strength.

Lacking most of the needed microstructural information, the synergic operation of the mechanisms described above cannot be fully accounted for in the model used here for the pre-assessment. This suggests that even though pure Copper had been regarded in the literature as a comparatively simple material for a case study, its creep-controlling mechanism, concurrent actions and interaction, and its dependence on temperature above 400 °C, are aspects that stills require investigation.

6. Conclusions

A modified version of the physically based Sandström model was used to obtain a pre-assessment of creep response for ETP copper under two different initial conditions, i.e., in the as-received state, a R240 half-hardened state, and after FSP. Subsequent experimental tests were carried out to

highlight the difference in the minimum creep rate dependence on the applied stress and temperature for the two investigated materials. The conclusions of this study can be summarised as follows:

i. The model curves obtained by introducing a few initial information, such as the grain size and the ultimate tensile strength at room temperature, in a set of constitutive equations, largely overlapped for the strain-hardened R240 and softer fine-grained FSP materials. This finding somewhat conflicted with the traditional view, which assumes that a fine grain size is an ineffective source of creep strengthening, if not detrimental.

ii. Creep testing carried out between 178 and 355 °C confirmed the picture provided by the pre-assessment. The softer FSP material underwent much higher strains upon loading and during primary creep, which, under constant load, led to much higher true stresses acting on the cross-sectional area of the sample. However, when reported as a function of the true stress, the minimum creep rate values for the two materials largely overlap on the same curves. Only at 355 °C did the FSP samples exhibit a somewhat higher creep rate when compared with the R240 samples and the pre-assessment curve.

iii. The experimental data obtained for R240 copper at 475 °C were not properly described by the physical model, as expected based on previous literature evidence.

The notable accuracy of the pre-assessment provided by the modified Sandström model and the non-negligible role of grain boundary strengthening in the low to intermediate temperature creep regime of pure metals highlighted in this study are definitely interesting findings that deserve to be considered in future studies.

Data availability

The raw data required to reproduce these findings are directly available in the tables of the present paper.

Appendix 1

The original formulation of the evolution of the dislocation density during straining can be expressed as [50,51]

$$\frac{d\rho}{d\varepsilon} = \frac{m}{bL} - \omega\rho - \frac{2}{\dot{\varepsilon}} M\tau_l\rho^2 \quad \text{(A1)}$$

where ω is a constant (ω =14.7 in pure Cu) and L is the dislocation mean free path (distance travelled by a dislocation before it undergoes a reaction) expressed, as

$$L = \frac{C_L}{\sqrt{\rho}} \quad \text{(A2)}$$

Combination of Eqns. (A1) and (A2) gives

$$\frac{d\rho}{d\varepsilon} = \frac{m\sqrt{\rho}}{bC_L} - \omega\rho - \frac{2}{\dot{\varepsilon}} M\tau_l\rho^2 \quad \text{(A3)}$$

In the original Sandström's terminology, the second term of the right-hand part of Eqn.(A3) expressed "dynamic recovery", while the third term represented the effects of "static recovery". While the "dynamic recovery" term is athermal, the "static recovery" term is strongly temperature-dependent through the dislocation mobility *M*, Eqn. (7). Thus, while at low temperatures, i.e. below 100°C, the "dynamic recovery" term is important in determining dislocation kinetics, as temperature decreases the third term becomes largely predominant, and for this reason and for the sake of simplicity, it has been here omitted, giving

$$\frac{d\rho}{d\varepsilon} = \frac{m\sqrt{\rho}}{bC_L} - \frac{2}{\dot{\varepsilon}} M\tau_l\rho^2 \quad \text{(A4)}$$

which, at steady state, where dislocation density is constant, gives

$$\dot{\varepsilon}_{ss} = \frac{2\tau_l bC_L}{m} M\left(\sqrt{\rho}\right)^3 \quad \text{(A5)}$$

The steady state dislocation density at steady state, from Eqn.(4), is

$$\rho = \left(\frac{\sigma_{\rho ss}}{\alpha mGb}\right)^2 \quad \text{(A6)}$$

that, combined with Eqn.(7), gives

$$\dot{\varepsilon}_{ss} = \frac{2\tau_l D_{0L} b^2 C_L}{mkT}\left(\frac{\sigma_{\rho ss}}{\alpha m G b}\right)^3 exp\left(\frac{\sigma_{\rho ss} b^3}{kT}\right) exp\left\{-\frac{Q_L}{RT}\left[1-\left(\frac{\sigma_{\rho ss}}{R_{max}}\right)^2\right]\right\} \qquad \text{(A7)}$$

References

[1] W.D. Jenkins, T.G. Digges, Creep of annealed and cold-drawn high-purity copper, J. Res. Natl. Bur. Stand. (1934). 47 (1951) 272–287. https://doi.org/10.6028/jres.047.035.

[2] O.D. Sherby, P.M. Burke, Mechanical behavior of crystalline solids at elevated temperature, Prog. Mater. Sci. 13 (1968) 323–390. https://doi.org/10.1016/0079-6425(68)90024-8.

[3] S. V. Raj, T.G. Langdon, Creep behavior of copper at intermediate temperatures-I. Mechanical characteristics, Acta Metall. 37 (1989) 843–852. https://doi.org/10.1016/0001-6160(89)90011-4.

[4] S. V. Raj, T.G. Langdon, Creep behavior of copper at intermediate temperatures-II. Surface microstructural observations, Acta Metall. Mater. 39 (1991) 1817–1822. https://doi.org/10.1016/0956-7151(91)90150-Y.

[5] S. V. Raj, T.G. Langdon, Creep behavior of copper at intermediate temperatures-III. A comparison with theory, Acta Metall. Mater. 39 (1991) 1823–1832. https://doi.org/10.1016/0956-7151(91)90151-P.

[6] W. Blum, J. Dvořák, P. Král, P. Eisenlohr, V. Sklenička, What is “stationary” deformation of pure Cu?, J. Mater. Sci. 49 (2014) 2987–2997. https://doi.org/10.1007/s10853-013-7983-4.

[7] R. Sandström, H.C.M. Andersson, The effect of phosphorus on creep in copper, J. Nucl. Mater. 372 (2008) 66–75. https://doi.org/10.1016/j.jnucmat.2007.02.004.

[8] R. Sandström, H.C.M. Andersson, Creep in phosphorus alloyed copper during power-law breakdown, J. Nucl. Mater. 372 (2008) 76–88. https://doi.org/10.1016/j.jnucmat.2007.02.005.

[9] R. Sandström, Basic model for primary and secondary creep in copper, Acta Mater. 60 (2012)

314–322. https://doi.org/10.1016/j.actamat.2011.09.052.

[10] R. Sandström, Influence of phosphorus on the tensile stress strain curves in copper, J. Nucl. Mater. 470 (2016) 290–296. https://doi.org/10.1016/j.jnucmat.2015.12.024.

[11] R. Sandström, F. Sui, Modeling of tertiary creep in copper at 215 and 250 °C, J. Eng. Mater. Technol. Trans. ASME. (2021). https://doi.org/10.1115/1.4049241.

[12] M.E. Kassner, M.-T. Pérez-Prado, Five-power-law creep in single phase metals and alloys., Prog. Mater. Sci. 45 (2000) 1–102.

[13] B. Wilshire, A.J. Battenbough, Creep and creep fracture of polycrystalline copper, Mater. Sci. Eng. A. (2007). https://doi.org/10.1016/j.msea.2006.08.094.

[14] G. Neumann, V. Tölle, C. Tuijn, Monovacancies and divacancies in copper, Phys. B Condens. Matter. (1999). https://doi.org/10.1016/s0921-4526(99)00209-4.

[15] R.S. Mishra, M.W. Mahoney, S.X. McFadden, N.A. Mara, A.K. Mukherjee, High strain rate superplasticity in a friction stir processed 7075 Al alloy, Scr. Mater. (1999). https://doi.org/10.1016/S1359-6462(99)00329-2.

[16] K. Surekha, A. Els-Botes, Development of high strength, high conductivity copper by friction stir processing, Mater. Des. (2011). https://doi.org/10.1016/j.matdes.2010.08.028.

[17] M. Barmouz, M.K.B. Givi, J. Jafari, Evaluation of tensile deformation properties of friction stir processed pure copper: Effect of processing parameters and pass number, J. Mater. Eng. Perform. (2014). https://doi.org/10.1007/s11665-013-0734-5.

[18] V.J. Arulmoni, R.M.S.R.S. Mishra, Friction Stir Processed Copper : A Review, Int. Res. J. Sustain. Sci. Eng. (2015).

[19] S. Cartigueyen, K. Mahadevan, Role of Friction Stir Processing on Copper and Copper based Particle Reinforced Composites – A Review, J. Mater. Sci. Surf. Eng. (2015).

[20] M. Ebrahimi, M.A. Par, Twenty-year uninterrupted endeavor of friction stir processing by focusing on copper and its alloys, J. Alloys Compd. (2019). https://doi.org/10.1016/j.jallcom.2018.12.083.

[21] V.E. Panin, R.W. Armstrong, Hall-Petch analysis for temperature and strain rate dependent deformation of polycrystalline lead, Phys. Mesomech. 19 (2016) 35–40. https://doi.org/10.1134/S1029959916010045.

[22] R.W. Armstrong, 60 years of hall-petch: Past to present nano-scale connections, Mater. Trans. (2014). https://doi.org/10.2320/matertrans.MA201302.

[23] R.P. Carreker, W.R. Hibbard, Tensile deformation of high-purity copper as a function of temperature, strain rate, and grain size, Acta Metall. (1953). https://doi.org/10.1016/0001-6160(53)90022-4.

[24] J. Lian, R.Z. Valiev, B. Baudelet, On the enhanced grain growth in ultrafine grained metals, Acta Metall. Mater. (1995). https://doi.org/10.1016/0956-7151(95)00087-C.

[25] B. Wu, B. Chen, Z. Zou, S. Liao, W. Deng, Thermal stability of ultrafine grained pure copper prepared by large strain extrusion machining, Metals (Basel). (2018). https://doi.org/10.3390/met8060381.

[26] I.M. Ghauri, M.Z. Butt, S.M. Raza, Grain growth in copper and alpha-brasses, J. Mater. Sci. (1990). https://doi.org/10.1007/BF01129942.

[27] M. Butt, P. Feltham, Grain growth in copper, Fiz. 14 (1982)149–153. (1982).

[28] I. Kaur, W. Gust, L. Kozma, Handbook of Grain and Interphase Boundary Diffusion Data, Ziegler Press, Stuttgart, 1989.

[29] T. Surholt, C. Herzig, Grain boundary self-diffusion in Cu polycrystals of different purity, Acta Mater. 45 (1997) 3817–3823. https://doi.org/10.1016/S1359-6454(97)00037-2.

[30] S. Spigarelli, R. Sandström, Basic creep modelling of Aluminium, Mater. Sci. Eng. A. 711 (2018) 343–349. https://doi.org/10.1016/j.msea.2017.11.053.

[31] Y. Kamimura, K. Edagawa, S. Takeuchi, Experimental evaluation of the Peierls stresses in a variety of crystals and their relation to the crystal structure, Acta Mater. 61 (2013) 294–309. https://doi.org/10.1016/j.actamat.2012.09.059.

[32] N. Nagata, S. Yoshida, Strain Rate and Temperature Dependence of the Flow Stress of Copper-Manganese Dilute Alloy Single Crystals, J. Japan Inst. Met. 32 (1968) 385–390. https://doi.org/10.2320/jinstmet1952.32.4_385.

[33] M. Regev, S. Spigarelli, A study of the metallurgical and mechanical properties of friction-stir-processed cu, Metals (Basel). 11 (2021) 656. https://doi.org/10.3390/met11040656.

[34] D. Angelova, S. Yankova, R. Yordanova, G. Atanasova, On monitoring mechanical characteristics of rolled electrolytic copper, in: Procedia Struct. Integr. 2, 2016: pp. 2315–2322. https://doi.org/10.1016/j.prostr.2016.06.290.

[35] D. Luo, C. Lu, L. Su, Microstructure and mechanical properties of pure copper subjected to skin pass asymmetric rolling, in: MATEC Web Conf. 185,00003, 2018. https://doi.org/10.1051/matecconf/201818500003.

[36] J. Jiang, T.B. Britton, A.J. Wilkinson, Evolution of dislocation density distributions in copper during tensile deformation, Acta Mater. 61 (2013) 7227–7239. https://doi.org/10.1016/j.actamat.2013.08.027.

[37] E. Schafler, M. Zehetbauer, T. Ungàr, Measurement of screw and edge dislocation density by means of X-ray Bragg profile analysis, Mater. Sci. Eng. A. 319–321 (2001) 220–223. https://doi.org/10.1016/S0921-5093(01)00979-0.

[38] W.D. Jenkins, T.G. Digges, C.R. Johnson, Tensile properties of copper, nickel, and 70-percent-copper-30-percent-nickel and 30-percent-copper-70-percent-nickel alloys at high

temperatures, J. Res. Natl. Bur. Stand. (1934). 58 (1957) 201–211. https://doi.org/10.6028/jres.058.027.

[39] Electrolytic Though-Pitch Copper Cu-ETP, Data sheet No. A1, Cons. Int. Pour Le Dev. Dui Cuivre Geneve. (1986).

[40] B. Wilshire, C.J. Palmer, Grain size effects during creep of copper, Scr. Mater. 46 (2002) 483–488. https://doi.org/10.1016/S1359-6462(01)01247-7.

[41] P. Kral, J. Dvorak, V. Sklenicka, T.G. Langdon, The characteristics of creep in metallic materials processed by severe plastic deformation, Mater. Trans. 60 (2019) 1506–1517. https://doi.org/10.2320/matertrans.MF201924.

[42] J. Dvorak, P. Kral, M. Svoboda, M. Kvapilova, V. Sklenicka, Enhanced creep properties of copper and its alloys processed by ECAP, in: IOP Conf. Ser. Mater. Sci. Eng. 63, 2014: p. 012141. https://doi.org/10.1088/1757-899X/63/1/012141.

[43] W. Blum, J. Dvořák, P. Král, P. Eisenlohr, V. Sklenička, Effect of grain refinement by ECAP on creep of pure Cu, Mater. Sci. Eng. A. 590 (2014) 423–432. https://doi.org/10.1016/j.msea.2013.10.022.

[44] E. Hersent, K. Marthinsen, E. Nes, On the effect of atoms in solid solution on grain growth kinetics, in: Metall. Mater. Trans. A Phys. Metall. Mater. Sci., 2014: pp. 4882–4890. https://doi.org/10.1007/s11661-014-2459-y.

[45] D. Caillard, J.L. Martin, New trends in creep microstructural models for pure metals, Rev. Phys. Appliquée. 22 (1987) 169–183. https://doi.org/10.1051/rphysap:01987002203016900.

[46] A. Manonukul, F.P.E. Dunne, Initiation of dynamic recrystallization under inhomogeneous stress states in pure copper, Acta Mater. 47 (1999) 4339–4354. https://doi.org/10.1016/S1359-6454(99)00313-4.

[47] G. Gottstein, Dynamic recrystallization of Cu single crystals during tensile deformation in creep, Met. Sci. 17 (1983) 497–502. https://doi.org/10.1179/030634583790420565.

[48] V.G. García, J.M. Cabrera, J.M. Prado, Role of Cu2O during hot compression of 99.9% pure copper, Mater. Sci. Eng. A. 488 (2008) 92–101. https://doi.org/10.1016/j.msea.2007.10.079.

[49] V.G. García, J.M. Cabrera, J.M. Prado, Modelling the hot flow stress of commercial purity coppers with different oxygen levels, in: Mater. Sci. Forum 426-432, 2003: pp. 3921–3926. https://doi.org/10.4028/www.scientific.net/msf.426-432.3921.

[50] R. Sandström, J. Hallgren, The role of creep in stress strain curves for copper, J. Nucl. Mater. 422 (2012) 51–57. https://doi.org/10.1016/j.jnucmat.2011.12.012.

[51] R. Sandström, The role of cell structure during creep of cold worked copper, Mater. Sci. Eng. A. 674 (2016) 318–327. https://doi.org/10.1016/j.msea.2016.08.004.

Table I. List of the most important parameters.

symbol	meaning	value [units]	ref
σ	true applied stress	[MPa]	-
s	engineering stress	[MPa]	-
$\dot{\varepsilon}_m$, $\dot{\varepsilon}_{ss}$	minimum or steady state creep rate	[s^{-1}]	-
α	constant	0.19	[8]
m	Taylor factor	3.06	[8]
R	gas constant	8.314 [J $mol^{-1}K^{-1}$]	-
G	shear modulus	4.75×10^4-17T [MPa]	[8]
b	Burgers vector	2.56×10^{-10} [m]	[8]
ρ	dislocation density	[m^{-2}]	-
σ_ρ	dislocation hardening term	$\alpha m G b \rho^{1/2}$ [MPa]	-
τ_l	dislocation line tension	$0.5Gb^2$ [N]	-
R_{max}	maximum strength at the testing temperature	[MPa]	-
k	Boltzmann constant	1.38×10^{-23} [J K^{-1}]	-
D_{0L}	pre-exponential factor in the Arrhenius self-diffusivity equation	1.3×10^{-5} [m^2s^{-1}]	[8]
Q_L	activation energy for self-diffusion	198 [kJ mol^{-1}]	[8]
Q_a	apparent activation energy for creep	[kJ mol^{-1}]	
UTS	room temperature tensile strength (engineering)	235 or 285 [MPa]	this study
C_L	strain hardening constant	57	[8]
G_T	shear modulus at the testing temperature	[MPa]	-
G_{RT}	shear modulus at room temperature	[MPa]	-
k_{HP}	Hall-Petch constant	[MPa $m^{-0.5}$]	-
β_0	constant	3.55×10^{-3} [K^{-1}]	[21]
β_1	constant	2×10^{-4} [K^{-1}]	[21]
B_{HP}	constant	91 [MPa^2 mm^{-1}]	[22]
d	grain size	[m]	-
d_0	initial grain size	3 or 10×10^{-6} [m]	this study
k_{GG}	grain growth parameter	3.6×10^{-8} [m^2 s^{-1}]	[27]
Q_{GG}	activation energy for grain growth	82 [kJ mol^{-1}]	[27]
D_{0GB}	pre-exponential factor in the Arrhenius grain boundary diffusion coefficient	[m^2 s^{-1}]	-
Q_{GB}	activation energy for grain boundary diffusion	[kJ mol^{-1}]	-
γ	grain boundary surface energy	0.625 [J m^{-2}]	[24]
Ω	atomic volume	1.3×10^{-29} [m^3]	[24]
δ	grain boundary width	1.0×10^{-9} [m]	[24]
t_m	time to minimum creep rate	[s]	-
U_p	interaction energy P atoms	8 [kJ mol^{-1}] at 100°C	[10]
σ_p	particle hardening term	[MPa]	-
d_p	particle diameter	[nm]	

Table II. Grain growth parameters from different sources.

k_{GG} [m^2 s^{-1}]	Q_{GG} [kJ mol^{-1}]	source
1.6×10^{-6}	84	[26]
3.6×10^{-8}	82	[27]
2.8×10^{-10}*	56	[25]

* calculated by Eqn. (11)

Table III. Examples of grain diffusivity parameters from different sources.

D_{0GB} [m^2 s^{-1}]	Q_{GB} [kJ mol^{-1}]	k_{GG} [m^2 s^{-1}]*	source
2.35×10^{-5}**	107**	1.2×10^{-4}	[28]
1.16×10^{-6}	85	6.0×10^{-6}	[29]

* calculated by Eqn. (12), values of the different parameters in Table I

** calculated from creep data

Table IV. Results of room temperature tensile tests (6 experiments)

material	Yield stress MPa]	UTS [MPa]	elongation [%]
parent sheet	225±5	285±8	36.7±0.4
FSP sheet	135±7.4	235±7	45.5±1.6

Table V. Summary of the creep results for R240 ETP copper (data from VLE in italic font).

test type	Temperature [C]	nominal stress [MPa]	minimum creep rate [s^{-1}]	true stress at minimum [MPa]
CLE	178	160	$1.3x10^{-8}$	182.7
CLE	178	180	$1.3x10^{-5}$	212.2
CLE	178	210	$2.4x10^{-3}$	269.8
CLE	252	120	$6.5x10^{-8}$	121.8
CLE	252	140	$5.3x10^{-7}$	160.7
CLE	252	150	$1.2x10^{-6}$	177.5
CLE	252	180	$1.3x10^{-4}$	213.1
CLE	355	55	$8.0x10^{-8}$	55.6
CLE	355	66	$1.5x10^{-7}$	66.9
CLE	355	85.5	$6.6x10^{-7}$	86.6
CLE	355	95	$7.0x10^{-5}$	131
VLE	*475*	*20*	*$5.0x10^{-8}$*	*21.1*
		41	*$5.2x10^{-6}$*	*46.1*
CLE	475	35	$1.1x10^{-6}$	38.1
CLE	475	55	$1.8x10^{-5}$	63.2
CLE	475	70	$1.7x10^{-4}$	86.9

Table VI. Summary of the creep results for FSP ETP copper (data from VLE in italic font).

test type	Temperature [C]	nominal stress [MPa]	minimum creep rate [s^{-1}]	true stress at minimum [MPa]
CLE	178	160	4.2×10^{-8}	202
VLE	*178*	*160*	*9.2×10^{-7}**	*178*
		138	*4.1×10^{-9}*	*154*
		171	*1.3×10^{-6}*	*204*
		160	*3.1×10^{-8}*	*193*
		193	*2.2×10^{-3}*	*255*
VLE	*178*	*170*	*3.5×10^{-7}*	*178*
		137	*1.8×10^{-9}*	*174*
		170	*4.6×10^{-7}*	*228*
CLE	178	180	1.0×10^{-4}	235
CLE	252	85	3.5×10^{-8}	90
VLE	*252*	*100*	*6.7×10^{-8}*	*104*
		90	*2.1×10^{-8}*	*95*
		100	*7.7×10^{-8}*	*106*
		150	*8.5×10^{-5}*	*172*
CLE	252	120	3.4×10^{-7}	136
CLE	252	130	3.5×10^{-7}	148
CLE	252	180	2.0×10^{-3}	216
CLE	355	45	2.8×10^{-7}	47
VLE	*355*	*50*	*4.0×10^{-7}*	*50*
		83	*8.0×10^{-6}*	*94*
CLE	355	55	3.8×10^{-7}	56
VLE	*355*	*70*	*1.9×10^{-6}*	*71*
		135.5	*1.9×10^{-3}*	*152*
CLE	355	90	1.9×10^{-5}	95
VLE	*355*	*100*	*1.4×10^{-5}*	*109*
		123	*7.1×10^{-5}*	*146*

* load change well in advance of attaining minimum creep rate range.

List of Figure Captions

Figure 1. Model curves for minimum creep rate as a function of applied stress at 355 and 178 °C, for pure copper with different tensile strength and grain size, calculated by supposing that the grain size remains stable during creep exposure.

Figure 2. Pre-assessment of the creep response of pure copper: material in R240 (half-hard state, *UTS*=285 MPa, grain size 10 μm) and after FSP (UTS=235 MPa, grain size 3 μm).

Figure 3. Comparison between the creep curves strain rate vs time, a) and c); strain rate vs strain, b) and d). The curves were obtained by testing R240 and FSP under the same experimental conditions: a) and b): 178 °C, 160 MPa; c) and d): 252 °C,120 MPa. In all the curves, the strain includes the deformation instantaneously accumulated upon loading.

Figure 4. Representative creep strain rate *vs.* strain curves at 252 °C. Numbers represent the nominal stress in MPa. In all the curves, the strain includes the deformation instantaneously accumulated upon loading.

Figure 5. Representative creep strain rate *vs*. strain curves at 475 °C for R240 samples. Numbers represent the nominal stress in MPa.

Figure 6. Hardness variation on R240 samples heads as a function of duration of the permanence at high T (heating and soaking times before loading where not considered). The broken lines represent the mean hardness of the R240 plate, and the relevant error band.

Figure 7. a) R240, CLE 355°C-55MPa, test duration 135 h; b) R240, CLE 475 °C-55 MPa, test duration 1.2 h; c) FSP, CLE 252 °C-85 MPa, overall test duration 655 h. Predicted grain sizes (Section 2.2) were: a) 52 μm; b) 20 μm; c) 24.5 μm.

Figure 8. TEM micrographs of crept samples: a) head, FSP crept at 355 °C (VLE tested under 50 and 83 nominal stresses, overall test duration 23 h; b) gauge length, R240 crept at 475 °C (VLE, tested under 20 and 41 nominal stresses, overall test duration 170 h). Insets in a) and b) show SAEDPs used to identify the crystallography of the detected oxides as Cu_2O.

Figure 9. Minimum creep rate as a function of true stress: a) R240 state; b) FSP state; c) comparison between the two datasets. Open and closed symbols in a) and b) represents VLE and CLE respectively.

Figure 10. Time to minimum creep rate as a function of minimum creep rate for R240 (open symbols) and FSP (closed symbols) states. The cross represent the datum from the curve at 250 °C-90 MPa in [9].

Figure 11. Yield stress and UTS as a function of testing temperature, obtained by a collection of different data, for Cu in annealed state [13,23,38,39]. The figure also plots the yield strength and UTS for a sheet cold-worked up to 6% and the trend of the *UTS* for a pure Cu rod with 21% cold work [39].

Figure 12. Comparison between pre-assessment curves and experimental data: R240 state; b. FSP state.

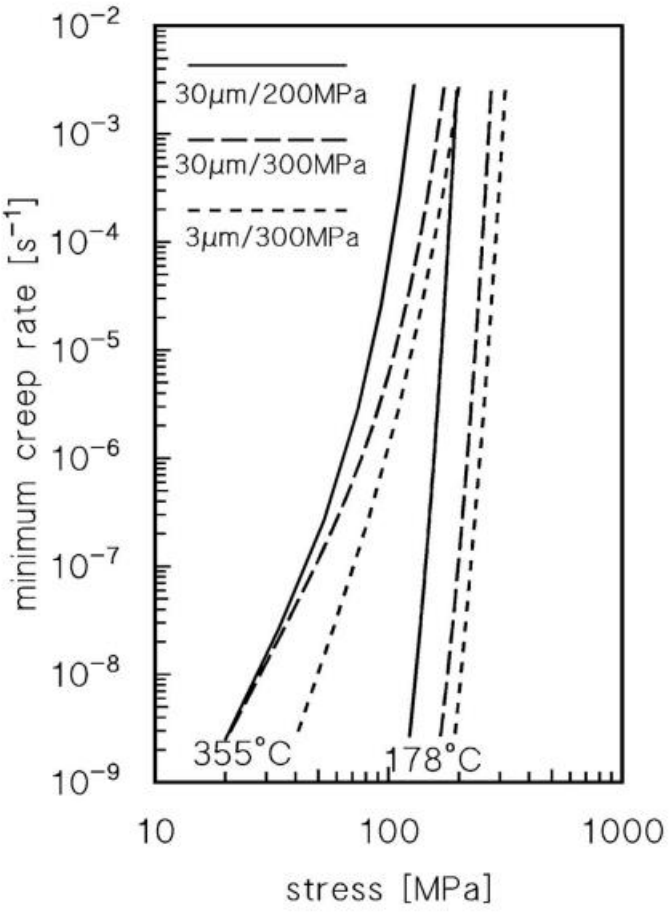
10^{-2}
10^{-3}
10^{-4}
10^{-5}
10^{-6}
10^{-7}
10^{-8}
10^{-9}
minimum creep rate [s^{-1}]
30µm/200MPa
30µm/300MPa
3µm/300MPa
355°C
178°C
10
100
1000
stress [MPa]

FIGURE 1

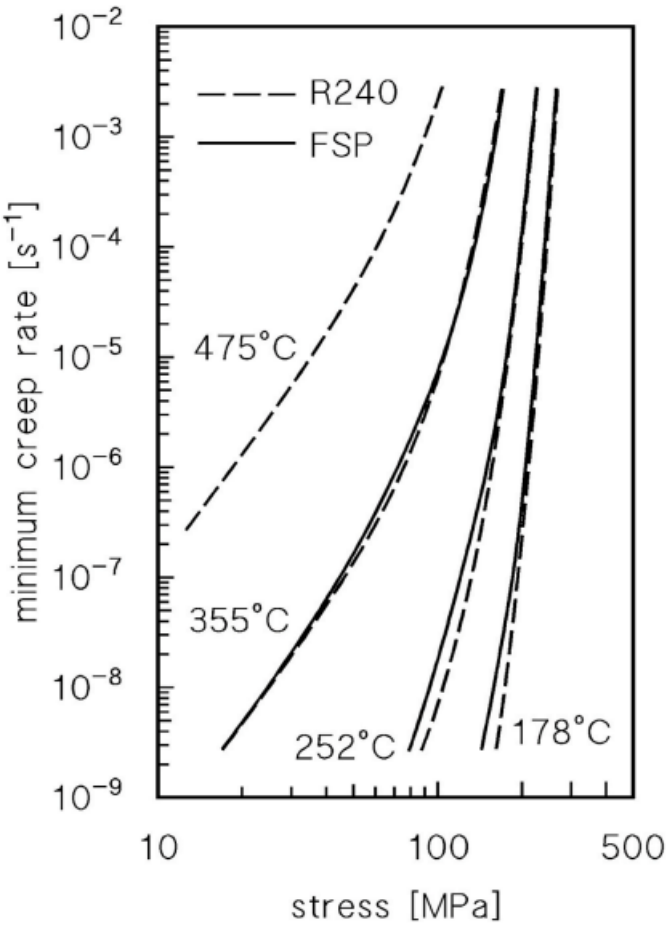
10^{-2}
10^{-3}
10^{-4}
10^{-5}
10^{-6}
10^{-7}
10^{-8}
10^{-9}
minimum creep rate [s^{-1}]
R240
FSP
475°C
355°C
252°C
178°C
10
100
500
stress [MPa]

FIGURE 2

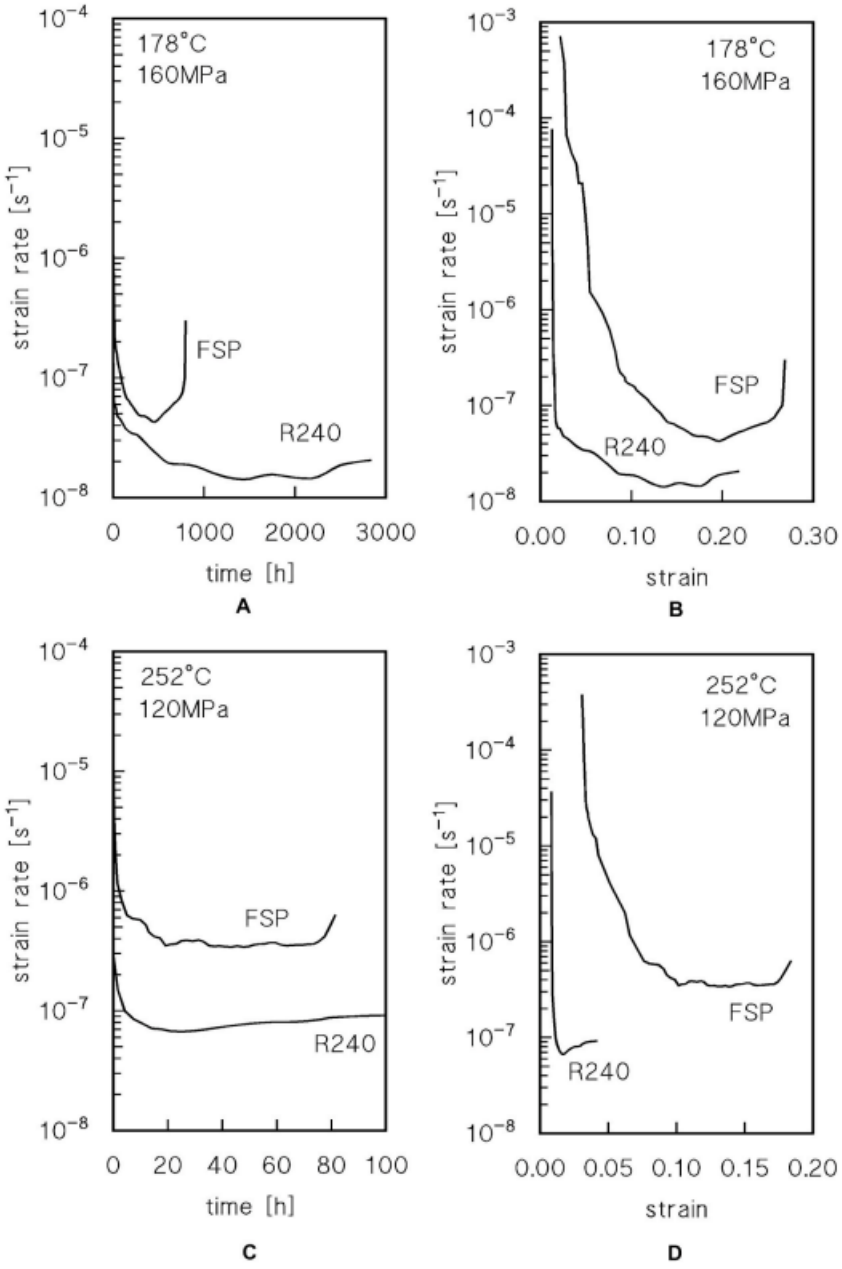
178°C
160MPa
FSP
R240
strain rate [s⁻¹]
time [h]
A
178°C
160MPa
FSP
R240
strain rate [s⁻¹]
strain
B
252°C
120MPa
FSP
R240
strain rate [s⁻¹]
time [h]
C
252°C
120MPa
FSP
R240
strain rate [s⁻¹]
strain
D

FIGURE 3

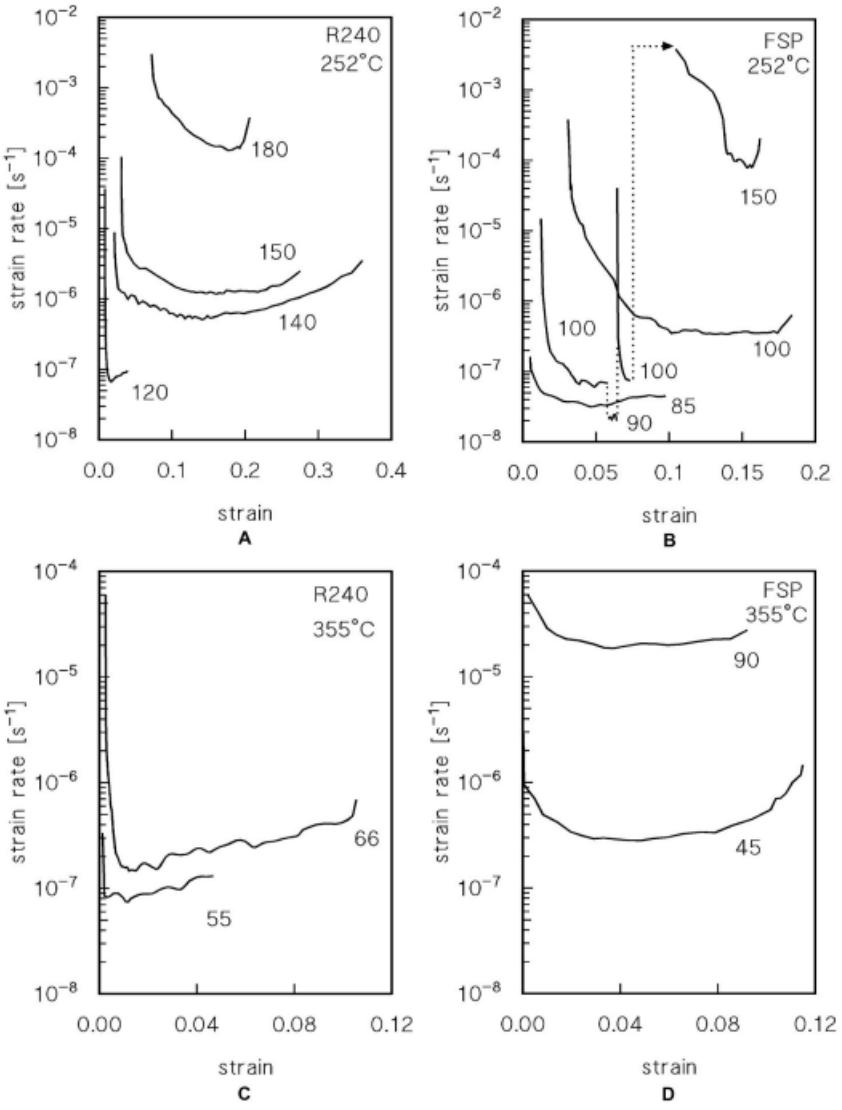
R240
252°C
180
150
140
120
strain rate [s⁻¹]
strain
A
FSP
252°C
150
100
100
100
90
85
strain rate [s⁻¹]
strain
B
R240
355°C
66
55
strain rate [s⁻¹]
strain
C
FSP
355°C
90
45
strain rate [s⁻¹]
strain
D

FIGURE 4

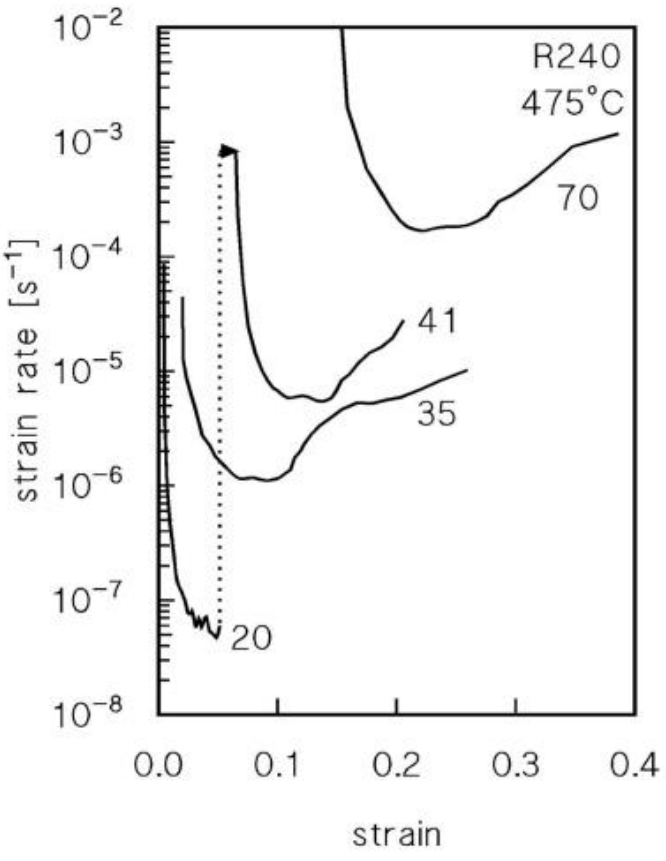

FIGURE 5

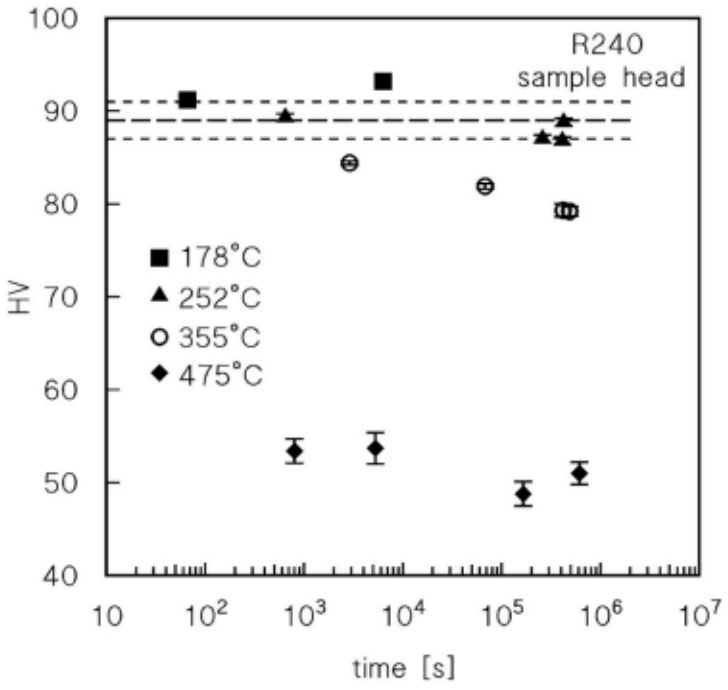

FIGURE 6

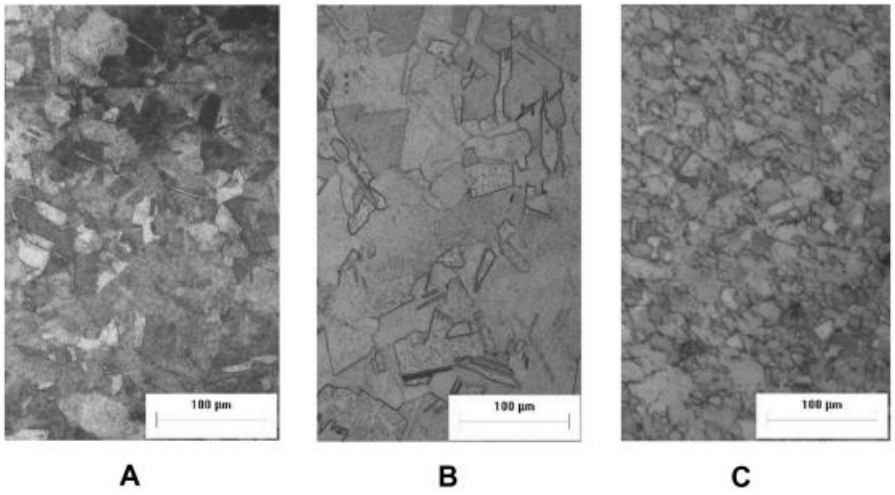

FIGURE 7

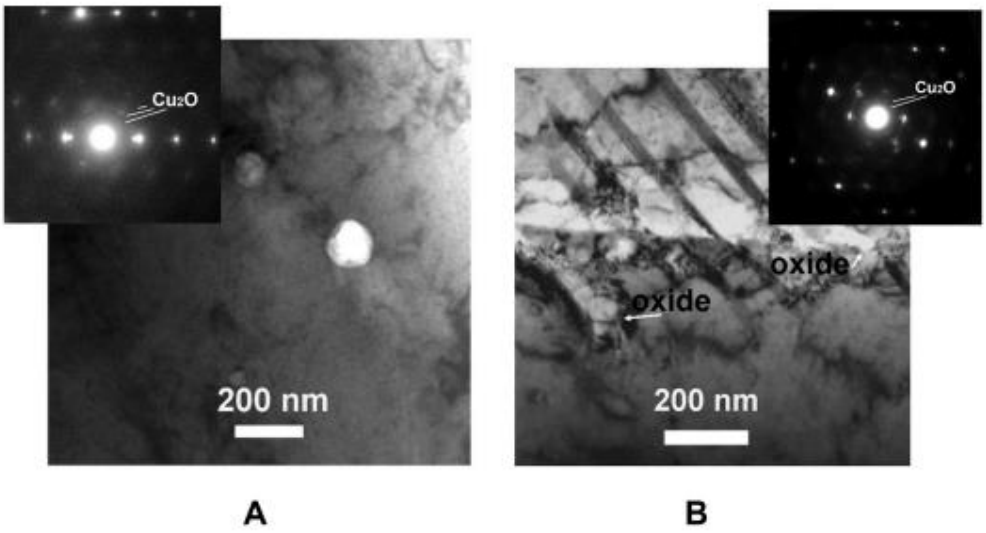

FIGURE 8

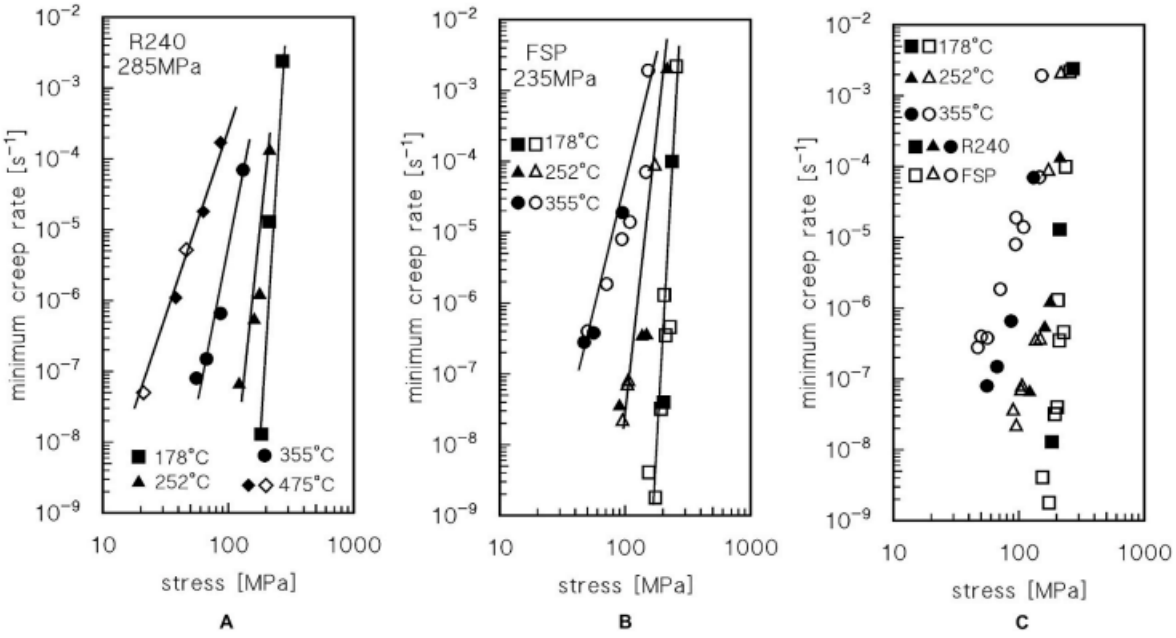

FIGURE 9

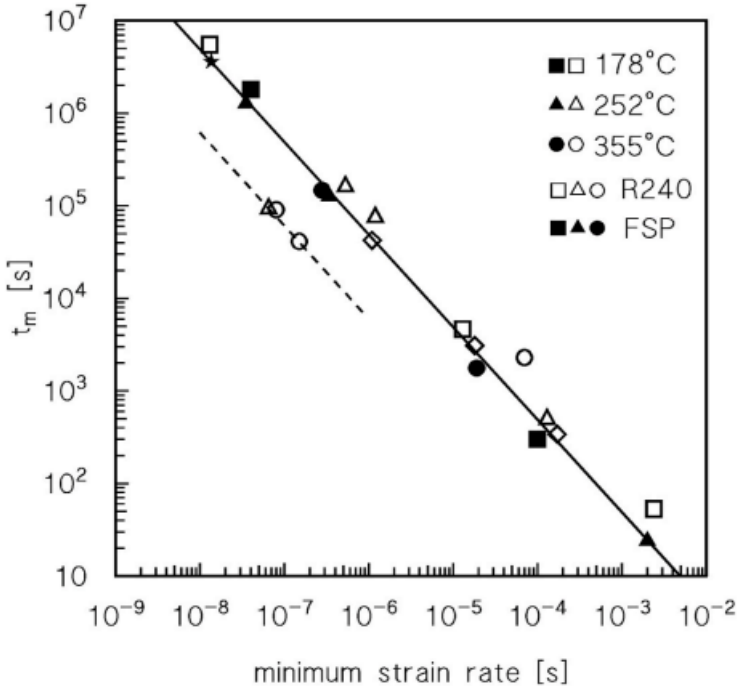

FIGURE 10

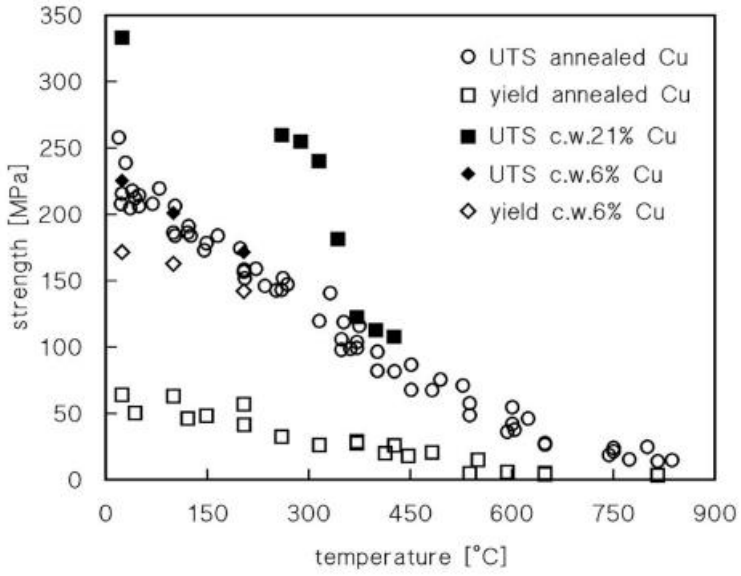

FIGURE 11

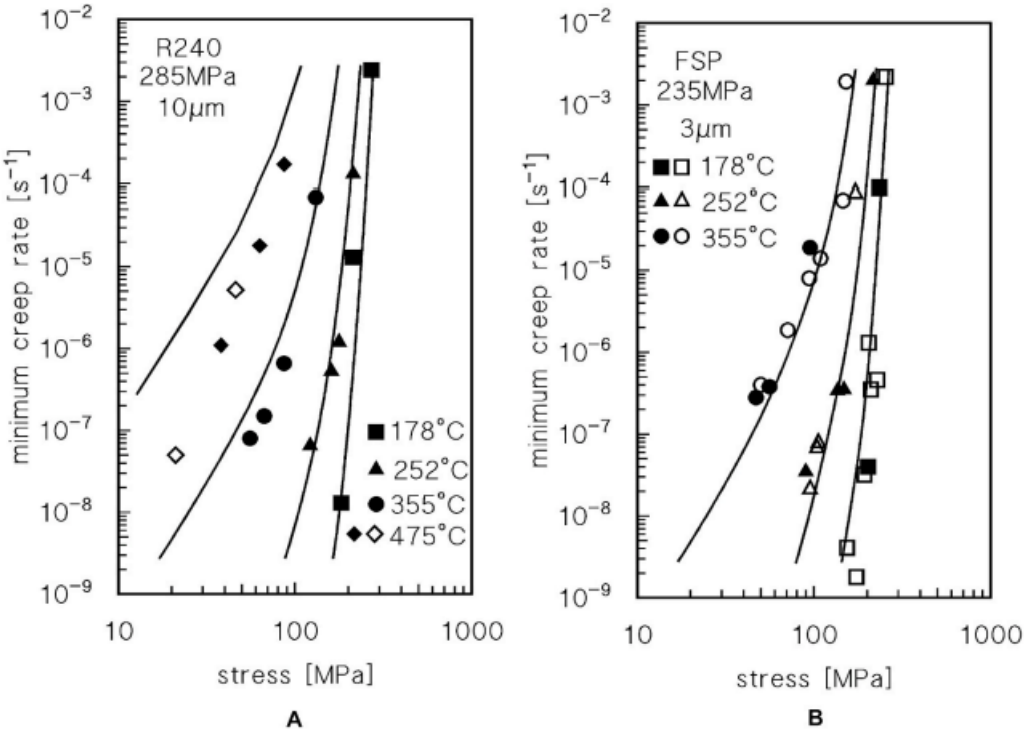
R240
285MPa
10μm
178°C
252°C
355°C
475°C
minimum creep rate [s⁻¹]
stress [MPa]
A
FSP
235MPa
3μm
178°C
252°C
355°C
minimum creep rate [s⁻¹]
stress [MPa]
B

FIGURE 12